FEDSM2013-16576

CAVITATION INVESTIGATION OF HYDROFOILS FOR MARINE HYDROKINETIC TURBINES

Ivaylo Nedyalkov [*]
Center for Ocean Renewable Energy
University of New Hampshire
Durham, New Hampshire 03824
Email: ipf2@unh.edu

Martin Wosnik
Center for Ocean Renewable Energy
University of New Hampshire
Durham, New Hampshire 03824
Martin.Wosnik@unh.edu

ABSTRACT

Three different hydrofoil sections were investigated in the recently renovated High-Speed Cavitation Tunnel (HICAT) at the University of New Hampshire: a NACA 0015 (reference foil), a NACA 63-424, and a bidirectional version of the NACA 63-424 hydrofoil. Bi-directional hydrofoils are of interest for marine renewable energy conversion, since they allow the elimination of pitch control mechanisms on marine hydrokinetic turbines. Hydrofoil lift and drag were measured for different velocities, pressures, and angles of attack. For some experimental conditions, comparative PIV measurements were performed in the near-wake region. A cavitation inception model for marine hydrokinetic turbines was derived. Cavitation numbers for inception were obtained for the two NACA 63-424 foils by varying pressure at constant speed as well as by varying speed at constant pressure. The performance of the NACA 63-424 and the bidirectional NACA 63-424 was compared.

NOMENCLATURE

c_D Coefficient of drag
c_L Coefficient of lift
c_L/c_D Lift over drag ratio
H Wave height
R Blade radius
U_∞ Free stream velocity
a axial induction factor
a' angular induction factor

d Water depth
k Wave number
p Local pressure
p_{atm} Atmospheric pressure
p_v Vapor pressure
p_{wave} Wave induced pressure
r Blade element distance from the hub center
v Free stream velocity
w_{rel} Relative velocity - no waves
$z_{hub}(t)$ Time-varying turbine hub submergence
α Hydrofoil angle of attack
λ Tip speed ratio
σ Cavitation number
ρ Density
φ Angle of rotation of the blade
θ Section pitch angle
ω Wave frequency

INTRODUCTION

Marine hydrokinetic turbines convert kinetic energy available in tidal, ocean or river currents. Power is proportional to swept area, and utility-scale turbines are destined to become quite large. At large diameters significant blade section and tip speeds can be reached, even at moderate rotation rates. Since these turbines operate in the proximity of a free surface, cavitation is a design consideration. If the cavitation behavior for the foil sections utilized in the turbine blades is known, then cavitation inception can be predicted for given turbine operating condi-

---

[*]corresponding author: ipf2@unh.edu

tions. The following operating parameters are considered in the proposed cavitation inception model: free stream velocity, tip speed ratio, angular and axial induction, water depth and wave height (which induce pressures and velocities), and rotor geometry and submergence.

Three hydrofoils were evaluated experimentally: NACA 0015, NACA 63-424, and a bidirectional version of NACA 63-424. The well-studied NACA 0015 foil was used as a base-line case. The NACA 63-424 is specified in the design of the Reference Horizontal Axis Turbine (RHAT) of the US Department of Energy. In marine renewable energy applications, simplicity of operation can be an advantage, and pitch control can be avoided by the use of bidirectional foils. Hence, a bidirectional version of the 63-424 foil was studied as well. This is a first step towards the goal of developing bi-directional foil sections that have favorable cavitation characteristics and minimize the inevitable loss in performance.

CAVITATION INCEPTION MODEL

Cavitation in marine horizontal axis turbines can be predicted if the cavitation inception behavior for the hydrofoil used in the turbine design is known, and the cavitation number for the blade at various span locations can be estimated. The cavitation number σ is defined as (e.g., [1]):

$$\sigma = \frac{p - p_v}{\frac{1}{2}\rho v^2}.$$ (1)

where p is the local static pressure, p_v is the vapor pressure at given water temperature, and $0.5\rho v^2$ is the dynamic pressure with local water velocity v.

For a blade element dr as shown in Fig. 1 the local static pressure p can be expressed in terms of the hydrostatic pressure, which depends on the blade element's position in its rotation $r\cos\varphi$ and on the time-varying submergence (tidal elevation or river stage) of the turbine hub $z_{hub}(t)$, as well as the wave induced pressure

$$p = p_{atm} - \rho g(z_{hub}(t) + r\cos\varphi) + p_{wave},$$ (2)

where the wave induced pressure was derived using linear wave theory (cf. [2]) as a function of wave height H and mean water depth d as

$$p_{wave} = \rho g \frac{H}{2} \frac{\cosh(k(d + z_{hub}(t) + r\cos\varphi))}{\cosh(kd)} \cos\vartheta,$$ (3)

where

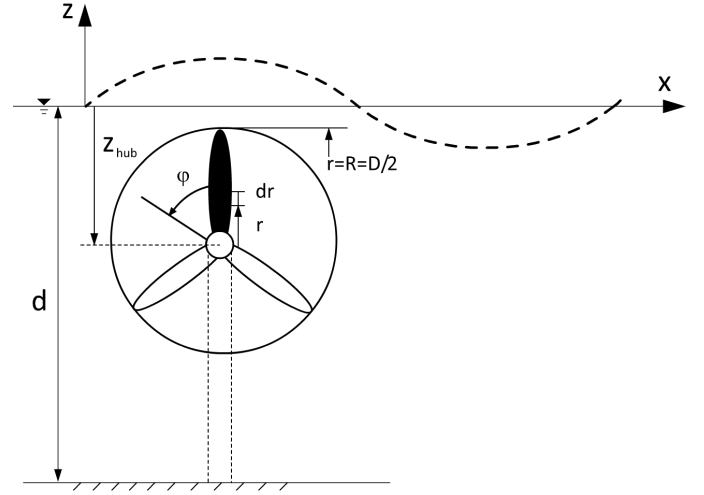$$\vartheta = (kx - \omega t).$$ (4)

FIGURE 1: SCHEMATIC OF A HORIZONTAL AXIS MARINE HYDROKINETIC TURBINE.

To calculate the local velocity in the dynamic pressure term in equation (1), we have to account for the relative velocity due to axial velocity and rotational motion of the blade (c.f. Fig. 2), and add to it the wave-induced velocities (c.f. Fig. 3). Turbine design codes are typically based on blade-element momentum (BEM) theory, which combines conservation of linear and angular momentum with calculation of forces on each blade element based on hydrofoil performance coefficients [3]. BEM codes calculate turbine operating conditions in terms of a linear induction factor, a, defined as the fractional decrease of free-stream velocity U_∞ at the rotor, and an angular induction factor a', which describes the induced fluid angular velocity as a fraction of rotor angular velocity. Fig. 2 shows a schematic of a horizontal-axis turbine blade section moving in the rotor plane. If we account for the angular and axial induction factors (a and a'), the angle of attack α and the relative velocity w_{rel} (in the absence of waves) are given by

$$\alpha = \arctan\left\{ \frac{1}{\lambda} \frac{(1-a)}{(1-a')} \right\} - \theta,$$ (5)

$$w_{rel} = U_\infty \left\{ (1+a')^2 \left(\frac{r}{R}\right)^2 \lambda^2 + (1-a)^2 \right\}^{1/2}.$$ (6)

where $\lambda \equiv \Omega R / U_\infty$ is the tip speed ratio, Ω is the angular velocity of the rotor, R radius of the rotor, U_∞ is the free-stream velocity, and θ is the section pitch angle of the blade.

If we want to estimate the minimum cavitation number, we have to compute the maximum velocity, which will occur when
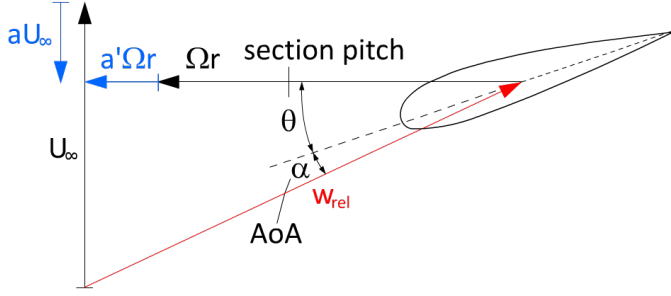
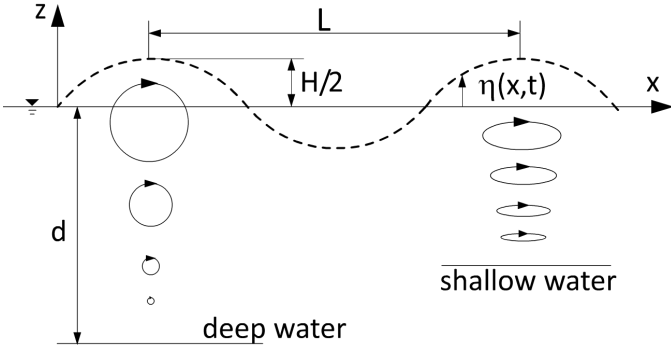**FIGURE 2**: RELATIVE VELOCITY OF THE TURBINE BLADE (TOP VIEW OF THE TURBINE).

FIGURE 3: TRAJECTORIES FOR WAVE INDUCED MOTION FOR DEEP AND SHALLOW WATER.

the vector of the wave-induced velocity is maximum and has the same direction as w_{rel}. It can be shown that the maximum wave-induced velocity at a given blade element is equal in magnitude to the horizontal velocity

$$\pm u_{wave} = \pm g\omega k \frac{H}{2} \frac{\cosh(k(d+z_{hub}(t)+r\cos\varphi))}{\cosh(kd)} \cos\vartheta, \quad (7)$$

for $\cos\vartheta = 1$ [2]. We used the $\pm$ sign since the waves can generally be oriented in any direction. In fact, the wave-induced pressure is minimum when $\cos\vartheta = -1$ so it will be convenient to use a negative sign in Eq. 7, in which case the minimum wave-induced pressure coincides in time with the maximum wave-induced velocity, for a given location.

The velocity v for the case of aligned w_{rel} and u_{wave} is then given by

$$\begin{aligned} v = & \ w_{rel} - u_{wave} \\ = & \ U_\infty \left\{ (1+a')^2 \left(\frac{r}{R}\right)^2 \lambda^2 + (1-a)^2 \right\}^{1/2} \end{aligned}$$

$$-g\omega k \frac{H}{2} \frac{\cosh(k(d+z_{hub}(t)+r\cos\varphi))}{\cosh(kd)} \cos\vartheta. \quad (8)$$

We can now express the cavitation number defined in equation 1 using pressure calculated with equations 2 and 3, and velocity calculated with equation 8. Cavitation can be avoided as long as

$$\sigma > \sigma_i \quad (9)$$

where σ_i is the experimentally determined value for cavitation inception for the particular hydrofoil. If we know σ_i, we can determine the limiting parameters at which a horizontal-axis marine turbine can operate without cavitation. The minimum cavitation number σ_{min} will occur at the tip of the blade, where the velocities are highest, when the tip is closest to the surface $\varphi = 0$, experiencing the lowest static pressure. This is also true when waves are present, since closer to the surface the wave-induced velocity is larger and the wave induced pressure can be minimum. Hence in order to evaluate σ_{min}, we should consider a blade element located at the tip of the blade.

EXPERIMENTAL SETUP

All the experiments were performed in the newly renovated HICAT (Fig. 4). The flow loop of HICAT was part of the original 1:6 scale physical model for the 36-inch Variable Pressure Cavitation Tunnel at David Taylor Model Basin (Carderock) built and tested at St. Anthony Falls Laboratory of the University of Minnesota [4], and was used in many fundamental cavitation studies in the past. The parts of the original tunnel were moved to the University of New Hampshire (UNH), where the tunnel was restored. Many new parts and features were designed and fabricated at UNH for the new tunnel to become HICAT, including a new contraction, test section, diffuser, motor, pressure/vacuum system, etc. The new contraction has an area ratio of 7:1 and a length over entrance diameter ratio of $L/D = 1.5$. The new test section has dimensions of $6'' \times 6'' \times 36''$ (0.15 m × 0.15 m × 0.91 m). The test section velocities can exceed 13 m/s, and velocity and pressure can be independently controlled [5]. The test section has optical access from all four sides and is equipped with a custom-designed lift and drag balance [6]. The balance provides simultaneous measurements of the lift and drag forces Fig. 5, and with its currently installed lift and drag members is capable of withstanding lift forces of up to 960 N and drag forces of up to 22 N.

HYDROFOILS

All data reported in this paper was obtained with hydrofoils of 75 mm chord length and 152 mm span. The leading edge is
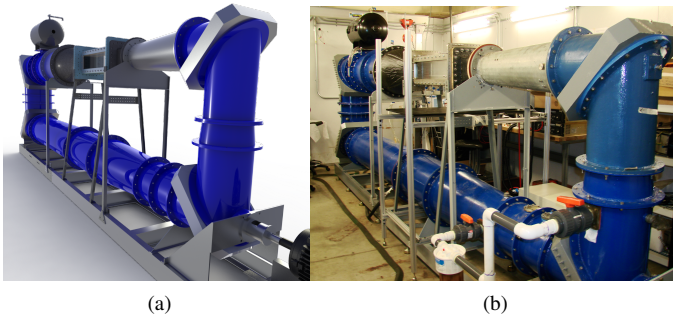
3

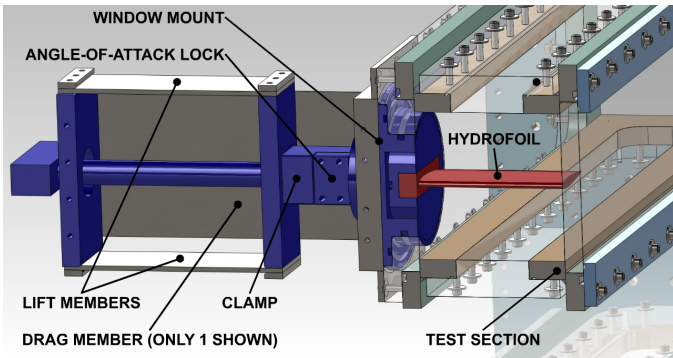**FIGURE 4**: THE RECENTLY RENOVATED HICAT: a) COMPUTER MODEL; b) PICTURE

FIGURE 6: HYDROFOIL SECTIONS. FROM TOP TO BOTTOM: NACA 0015; NACA 63-424; BIDIRECTIONAL FOIL.

LIFT AND DRAG MEASUREMENTS

The NACA 0015 foil was tested first. The test section speed was set to 2, 3, 4 and 5 m/s and at each speed setting the angle of attack was changed from 0 to 20 degrees with increments of 2 degrees. The water level in the riser tank was set to approximately 0.5 m above the foil and the tunnel was open to atmosphere. Hence, the gauge pressure in the test section varied with speed, from approximately 3 to -8 kPa. Lift and drag measurements were performed at each setting and coefficients of lift and drag were computed (Fig. 7 and Fig. 8) and compared to NACA 0015 foil data from Sheldahl and Klimas (1981) [8].

The lift coefficient data agree better at lower angles of attack. At larger angles of attack both lift and drag forces on the foil will increase in the HICAT, due to blockage effects. However, the significant drag increase when the flow begins to separate on the suction side between angles of attack of 13 degrees to 16 degrees was well captured, as can be seen from comparison of the data sets for Reynolds numbers of 150,000 and 375,000 with the Sandia data for 160,000 and 360,000 in Fig. 8. Overall, it should be noted that the drag measurements are less accurate than the lift measurements. Note that no blockage corrections were applied to the data presented here.

Next, the unidirectional and bidirectional NACA 63-424 foils were tested at the same speeds (2, 3, 4, and 5 m/s). At each speed setting, the pressure at the foil level in the test section was independently set to -10, 0 and 10 kPa gauge pressure. For each of these settings, the angle of attack was varied from 0 to 20 degrees with increments of 2 degrees.

For all speed settings, a dependence of results on test section pressure was noticed. The coefficient of lift is mostly higher for lower test section pressures, c.f. Fig. 9, however, there was no clear trend for the differences in drag coefficient at various pressures in Fig.10. The reason for the pressure dependence likely stems from the pressure difference between the inside and outside of the test section on a flexible seal installed in the new balance, and will be addressed in a redesign of the seal. For
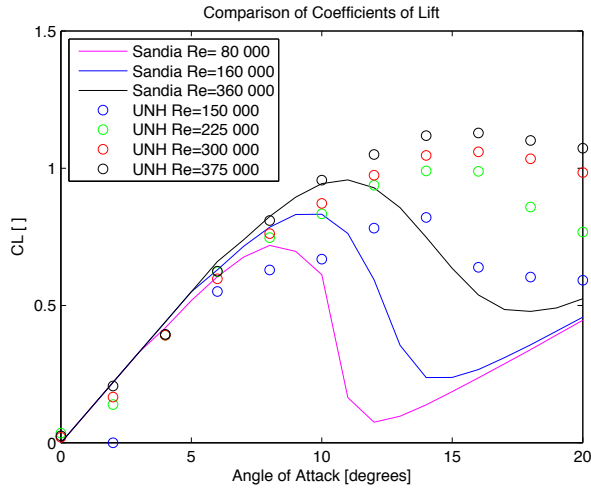

FIGURE 5: RENDERING OF FORCE BALANCE WITH HYDROFOIL INSTALLED IN TEST SECTION, LOOKING DOWNSTREAM.

159 mm downstream of the end of the contraction/beginning of the test section. The NACA 0015 hydrofoil is a symmetric foil with maximum thickness of 15% chord. The NACA 63-424 foil is a 6-series NACA foil. The 3 denotes the chordwise position of minimum pressure in tenths of chord from the leading edge, the 4 after the dash gives the design lift coefficient in tenths, and the last two digits (24) again indicate thickness in percent chord [7]. The bidirectional foil was created using the upstream part of the NACA 63-424 up to the location of maximum thickness. This part was mirrored vertically, and flipped along the horizontal axis, thus creating a new downstream part. The new "trailing edge" was moved to the appropriate chord distance, and shifted vertically until both parts could be connected via tangents at maximum thickness. The bi-directional version of the NACA 63-424 achieved about 80% of $(c_L/c_D)_{max}$ of the NACA 63-424 when compared using javafoil [6]. The shapes of all three foils are shown in Fig. 6.

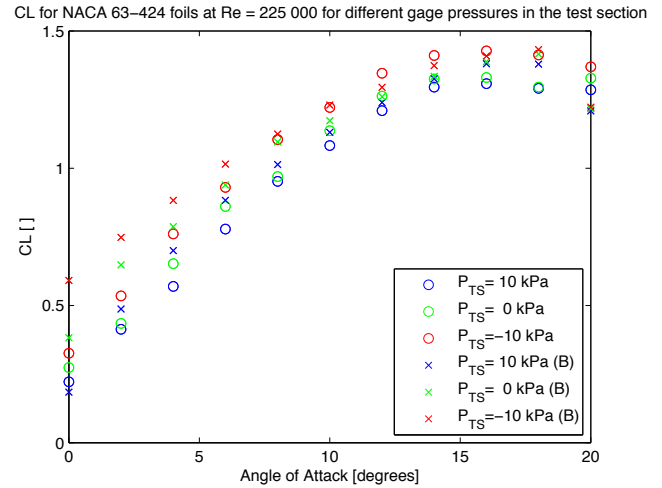**FIGURE 7**: COMPARISON OF COEFFICIENTS OF LIFTS FOR NACA0015 FOIL.

FIGURE 9: COMPARISON OF COEFFICIENTS OF LIFT FOR NACA 63-424 FOILS FOR A GIVEN SPEED AT VARIOUS PRESSURES.
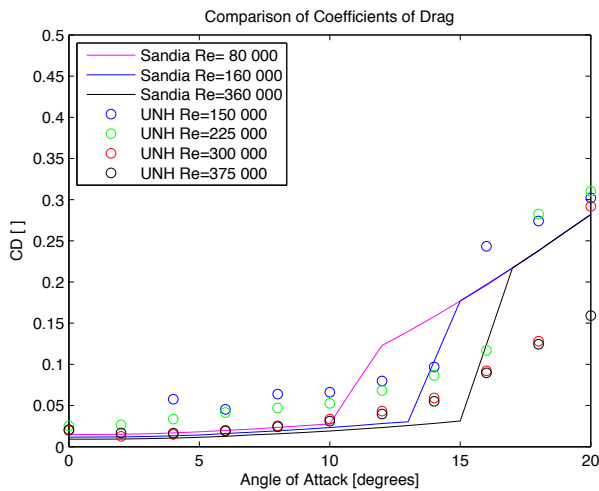

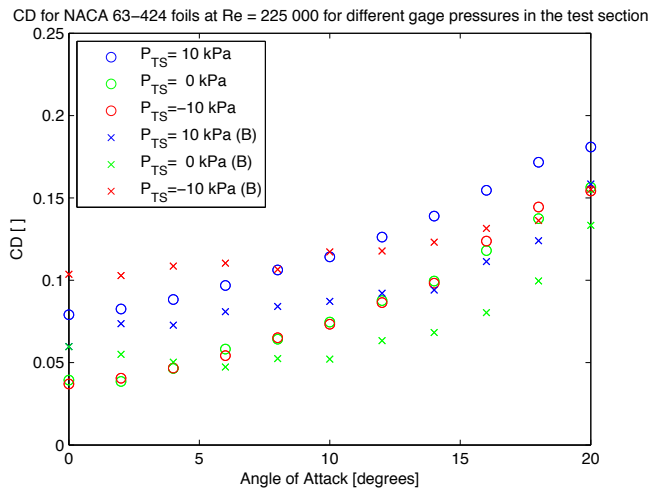**FIGURE 8**: COMPARISON OF COEFFICIENTS OF DRAG FOR NACA0015 FOIL.

FIGURE 10: COMPARISON OF COEFFICIENTS OF DRAG FOR NACA 63-424 FOILS FOR A GIVEN SPEED AT VARIOUS PRESSURES.

Figures 11 through 13 the results for -10, 0 and 10 kPa gauge pressure were averaged for each Reynolds number.

For the (unidirectional) NACA 63-424 foil the lift coefficients are similar over the range of Reynolds number investigated, except at high angles of attack, where higher Reynolds numbers correspond to higher lift coefficients. For the bidirectional NACA 63-424 foil, however, there is a notable decrease of lift coefficient with increasing Reynolds number Fig.11, which is not desirable. Nevertheless, both foils have similar coefficients. The drag of the bidirectional foil is higher at lower angles of attack, and lower at higher angles of attack, compared to the drag

of the unidirectional foil Fig.12. Also, for both foils, the drag is decreasing with increasing Reynolds number. As a results, the c_L/c_D ratio is higher at higher Reynolds numbers for both foils Fig. 13. This trend is more prominent for the unidirectional foil. Thus, the bidirectional foil has higher c_L/c_D ratio compared to the unidirectional foil only at lower Reynolds numbers. Lift and drag coefficients are only used for qualitative comparisons between foils here, since the data were not blockage-corrected.
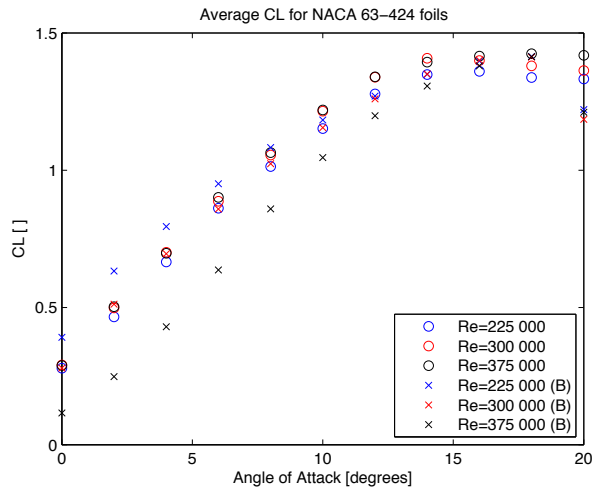
5

FIGURE 11: COMPARISON OF COEFFICIENTS OF LIFT BETWEEN THE UNIDIRECTIONAL AND BIDIRECTIONAL NACA 63-424 FOILS FOR VARIOUS REYNOLDS NUMBERS.
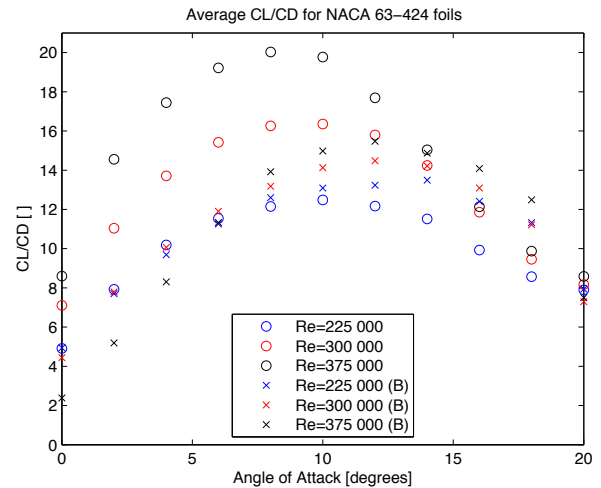

FIGURE 12: COMPARISON OF COEFFICIENTS OF DRAG BETWEEN THE UNIDIRECTIONAL AND BIDIRECTIONAL NACA 63-424 FOILS FOR VARIOUS REYNOLDS NUMBERS.

PIV MEASUREMENTS

PIV measurements were performed for both 63-424 foils at angles of attack of 4, 8 and 12 degrees, and for each angle, the speed was set to 4, 6, 8 and 10 m/s. For each measurement, 1,000 images were taken at a frequency of 3,600 frames per second. Sample contour plots can be seen in Fig.14 and Fig.15, for a test section speed of 8 m/s and a Reynolds number of 600,000.

FIGURE 13: COMPARISON OF COEFFICIENTS OF LIFT DIVIDED BY COEFFICIENTS OF DRAG BETWEEN THE UNIDIRECTIONAL AND BIDIRECTIONAL NACA 63-424 FOILS FOR VARIOUS REYNOLDS NUMBERS.
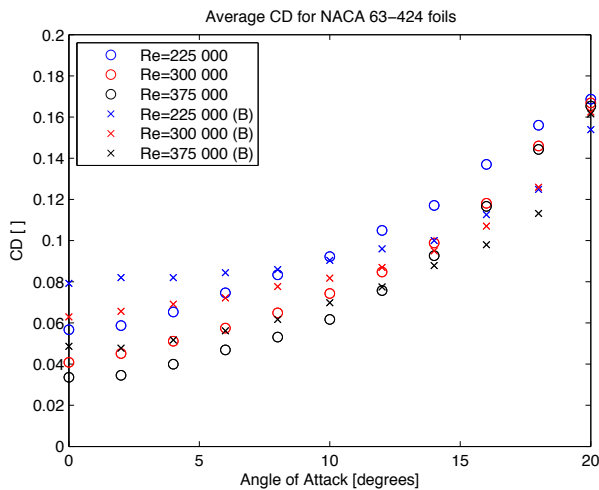
Fig. 16 compares velocity profiles in the near-wake of both foils, approximately 25mm downstream of the trailing edge. The velocity deficit for the bidirectional foil is larger than the one for the unidirectional foil. This is also the case for the other two angles of attack for the speed setting of 8 m/s, suggesting that for these angles, the drag on the bidirectional foil is larger than that on the unidirectional foil. This is consistent with the results at lower Reynolds number shown in Fig. 12.

CAVITATION INCEPTION

Cavitation inception was observed for the unidirectional and bidirectional NACA 63-424 foils. The tests were conducted at temperatures in the range 25.5 to 24.5°C for the bidirectional foil and 25 to 23.5°C for the unidirectional foil. The dissolved oxygen content in the water was measured with a Hydrolab DS5 probe, and was between 5.5 and 5.7 ppm for the bidirectional foil tests and between 4.8 and 5.3 ppm for the unidirectional foil tests.

The results for the cavitation inception experiments are shown in Fig. 17. First, the bidirectional foil was tested at 8 m/s and the cavitation number was varied by varying the pressure in the test section. The cavitation numbers for inception were obtained for angles of attack between -4 and 12 degrees, and the cavitation numbers for desinence were obtained for the positive angles of attack. The cavitation numbers for inception at -4, 4 and 12 degrees were also obtained at constant test section pressure of 52 kPa (absolute pressure), while slowly varying test section velocity. The percentage differences for the inception

cavitation numbers obtained this way were +8.7, +4.5, and +8.4.

Next, the unidirectional foil was tested at angles of attack between -7 and 12 degrees. The test section velocity was again set to 8 m/s and the pressure was varied to obtain cavitation numbers for inception. At negative angles of attack, cavitation was observed to occur on *both sides* of the foil at similar cavitation numbers. As the angle of attack was decreased from -2 to -7 degrees, the cavitation inception occurred at higher cavitation numbers on the pressure surface, but at lower cavitation numbers on the suction surface. The cavitation numbers for inception at -5, 4 and 12 degrees were also obtained by varying test section velocity while pressure in the test section remained constant at 51 kPa (absolute pressure). The percentage differences for the inception cavitation numbers obtained this way were +7.5, +2.1 and -0.4.

Non-symmetry in the cavitation inception with respect to zero degree angle of attack was observed for both foils, with non-symmetry being more noticeable for the unidirectional foil. Both foils have similar cavitation characteristics in the range of -4 to 12 degrees angle of attack, although the bidirectional foil cavitated at slightly lower cavitation numbers.
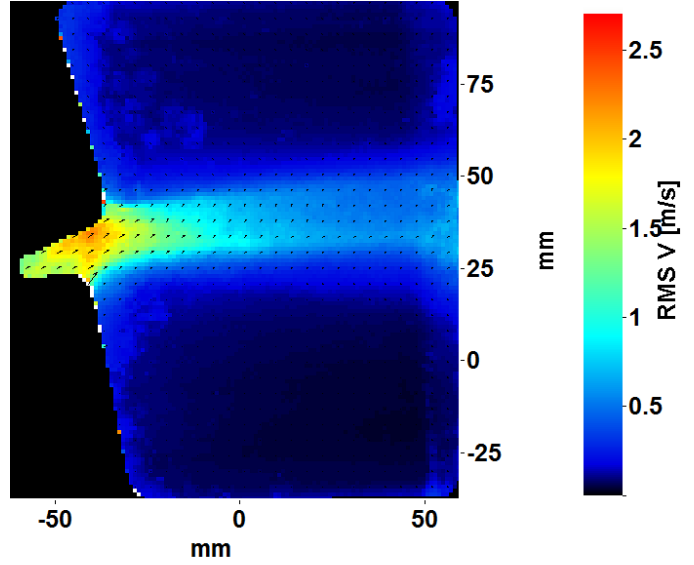

FIGURE 15: CONTOUR OF THE RMS OF VELOCITY FLUCTUATIONS IN THE WAKE OF THE UNIDIRECTIONAL NACA 63-424 FOIL AT 12 DEGREES ANGLE OF ATTACK AND 8 m/s FREE STREAM VELOCITY.
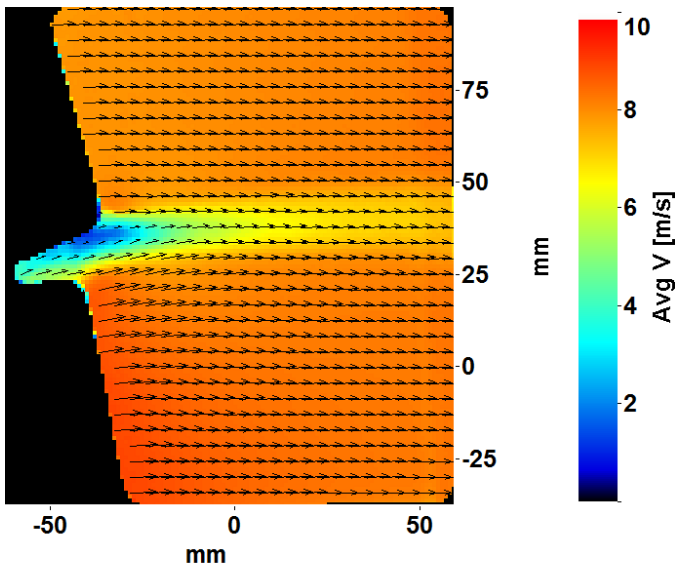

FIGURE 14: AVERAGE VELOCITY CONTOUR IN THE WAKE OF THE UNIDIRECTIONAL NACA 63-424 FOIL AT 12 DEGREES ANGLE OF ATTACK AND 8 m/s FREE STREAM VELOCITY.
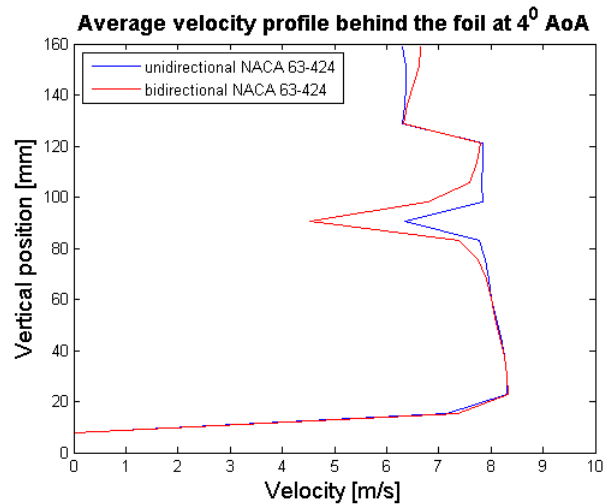

FIGURE 16: VELOCITY PROFILES BEHIND THE NACA 63-424 FOILS AT 4 DEGREES ANGLES OF ATTACK AND FREE STREAM VELOCITY OF 8 m/s.
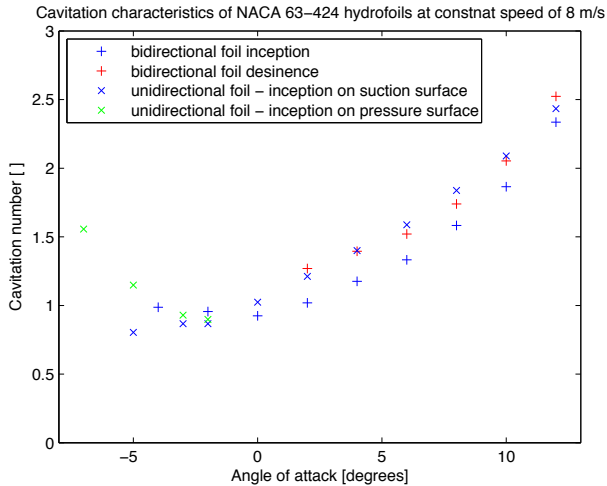
7

FIGURE 17: CAVITATION CHARACTERISTICS FOR THE UNIDIRECTIONAL AND BIDIRECTIONAL NACA63-424 FOILS.

SUMMARY

Three different hydrofoil sections were investigated in the recently renovated High-Speed Cavitation Tunnel (HICAT) at the University of New Hampshire: a NACA 0015 (reference foil), a NACA 63-424 and a bidirectional version of the NACA 63-424 hydrofoil.

Lift and drag were measured for different velocities, pressures, and angles of attack, and PIV measurements were performed in the near-wake region. A cavitation inception model for marine hydrokinetic turbines was derived. It requires input in the form of the inception cavitation number σ_i to determine the limiting parameters at which a horizontal-axis marine turbine can operate without cavitation. Inception and desinence cavitation numbers were then obtained experimentally for the unidirectional and bidirectional 63-424 foils. In non-cavitating regimes, the bidirectional foil has similar lift characteristics as the unidirectional foil (especially at lower Reynolds numbers) but has slightly higher drag, especially in the range from 0 to 10 degrees angle of attack. However, the bidirectional foil cavitates at slightly lower cavitation numbers, which would allow its use closer to the water surface, or at higher tip speed ratio for the same submergence. The latter would increase the performance of the the bidirectional foil. The results to date suggest that the use of the bidirectional 63-424 foil instead of the unidirectional foil may be beneficial for marine renewable energy conversion, where pitch control of the blades would require additional complexity and maintenance of the machinery.

REFERENCES

[1] Knapp, R., Daily, J., and Hammitt, F., 1979. *Cavitation*. Institute of Hydraulic Research, University of Iowa.
[2] Dean, R., and Dalrymple, R., 1991. *Water Wave Mechanics for Engineers and Scientists*. World Scientific.
[3] Manwell, J., McGowan, J., and Rogers, A., 2002. *Wind Energy Explained: Theory, Design and Application*. John Wiley & Sons.
[4] Purdy, H. D., and Straub, L. G., 1948. Model Experiment for the Design of a Sixty Inch Water Tunnel. Tech. Rep. 10,11,12,13,14,15, St. Anthony Falls Hydraulic Laboratory University of Minnesota.
[5] Nedyalkov, I., 2012. "Design of Contraction, Test Section, and Diffuser for a High-Speed Water Tunnel". MS Thesis, Chalmers University of Technology.
[6] Therrien, R., Roux, S., and Comtois, B., 2012. Design of a High Speed Water Tunnel Force Balance & Testing of High Performance Hydrofoils for Marine Hydrokinetic Turbines. Tech. rep., University of New Hampshire.
[7] Abbott, I. H., and von Doenhoff, A. E., 1959. *Theory of Wing Sections*. Dover Publications.
[8] Sheldahl, R. E., and Klimas, P. C., 1981. Characteristics of Seven Airfoil Sections Through 180 Degrees Angle of Attack for Use in Aerodynamic Analysis of Vertical Axis Wind Turbines. Tech. Rep. SAND80-2114, Sandia National Laboratories, Albuquerque, New Mexico.